NANO LETTERS

pubs.acs.org/NanoLett Letter

Adhesion of 2D MoS_2 to Graphite and Metal Substrates Measured by a Blister Test

Metehan Calis, David Lloyd, Narasimha Boddeti, and J. Scott Bunch*

Cite This: *Nano Lett.* 2023, 23, 2607−2614 Read Online

ACCESS | Metrics & More | Article Recommendations | Supporting Information

ABSTRACT: Using a blister test, we measured the work of separation between MoS_2 membranes from metal, semiconductor, and graphite substrates. We found a work of separation ranging from 0.11 ± 0.05 J/m^2 for chromium to 0.39 ± 0.1 J/m^2 for graphite substrates. In addition, we measured the work of adhesion of MoS_2 membranes over these substrates and observed a dramatic difference between the work of separation and adhesion, which we attribute to adhesion hysteresis. Due to the prominent role that adhesive forces play in the fabrication and functionality of devices made from 2D materials, an experimental determination of the work of separation and adhesion as provided here will help guide their development.

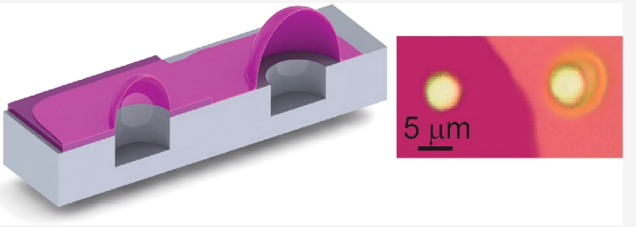

KEYWORDS: *two-dimensional material adhesion, MoS_2 on graphite, MoS_2 on gold, Young's modulus, work of separation, work of adhesion*

Two-dimensional (2D) materials[1] possess both remarkable mechanical properties[2−4] such as high tensile strength and impermeability[5,6] to gases and extraordinary electrical and thermal properties such as high thermal conductivities,[7,8] large charge carrier mobilities,[9,10] and band gaps tunable by strain.[11] While initial research on 2D materials focused on graphene, more recently this has been extended to 2D semiconductors such as transition-metal dichalcogenides (TMDCs).[12] Combining different 2D materials to fabricate heterostructure devices[13,14] and using 2D single layers as building blocks,[15] more complex devices with advanced functionality are created.[16−18] Manufacturing of electrical and mechanical devices from 2D materials typically requires that the 2D layers are transferred to substrates and in the case of heterostructure devices the transfer involves stacking dissimilar 2D materials on top of each other.[19] The fabrication and performance, therefore, depend critically on the interfacial adhesion between the 2D materials and the surface it is in contact with. For this reason, understanding and controlling interfacial adhesion is of paramount importance.[20,21]

One of the most well-studied TMDCs is atomically thin MoS_2, which possesses exceptional mechanical strength,[22] flexibility,[23] high carrier mobility,[24] and a strain-tunable band gap.[25] While the adhesion of MoS_2 to various substrates such as other 2D materials and metals[21,26,27] has been previously studied, these studies have been limited to nanoscale areal regions or centimeter size surfaces. Though both the nanoscale and macroscopic techniques offer unique insights into the delamination mechanics, these techniques may not be directly applicable to adhesion involved in delamination at the microscale where many devices from 2D materials operate.

Here, we use the constant-N pressurized blister test[28] to measure the work of separation and the work of adhesion of MoS_2 from metal, semiconductor, and graphite substrates. The constant-N pressurized blister test was previously used to determine the Young's modulus,[29] adhesion energy,[30] and shear stress[31,32] of atomically thin 2D membranes. The ease of sample preparation and straightforward experimental configuration make this test ideally suited for such measurements at the microscale. Metals, semiconductor, and graphite are chosen as substrate materials because of their dissimilar electrical,[26−28,33,34] mechanical,[29,30] and optical[31,32] properties and their ubiquity as substrates for 2D material devices.[35−38]

The blister test uses an applied pressure difference across a 2D membrane suspended over cylindrical microcavities.[29,30,39] For these experiments, we create etched cylindrical cavities on an oxidized silicon surface which is then coated with a metal or semiconductor such as gold (Au), chromium (Cr), titanium (Ti), germanium (Ge), or graphite. To fabricate the metal and Ge substrates, we pattern the silicon oxide (SiO_x)/silicon (Si) wafer with cylindrical microcavities using photolithography. Metal or Ge is evaporated over the substrate to form a thin film. Subsequently, chemical vapor deposition (CVD) grown MoS_2 flakes are transferred over the well to seal the microcavities (Figure 1a). To fabricate graphite wells, we

Received: December 14, 2022
Revised: March 30, 2023
Published: April 3, 2023

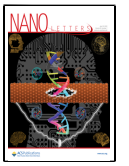

https://doi.org/10.1021/acs.nanolett.2c04886
Nano Lett. 2023, 23, 2607−2614

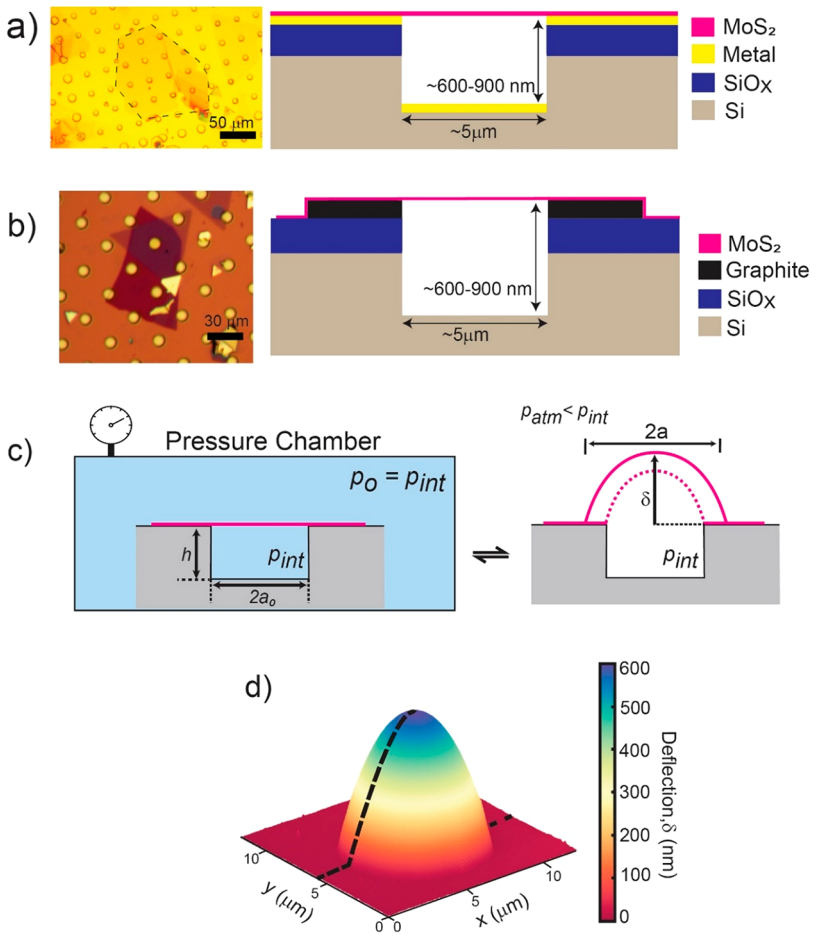

Figure 1. (a) (left) Optical image of MoS_2 over a gold substrate. The dashed lines show the boundary of the MoS_2 flakes. (right) Schematic image of the device with the gold substrate. (b) (left) Optical image of MoS_2 over a graphite substrate and (right) a schematic of the device. (c) Schematic illustration of the experimental procedure. Devices are placed into a pressure chamber and kept until $p_0 = p_{int}$. When the devices are taken out, the membrane bulges up due to $p_{int} > p_{ext}$ ($\sim p_{atm}$). This process is then repeated until the delamination. (d) AFM image of the blister. The dashed line represents a line cut passing through the center of the blister, from which the maximum deflection and radius are obtained.

start with the mechanical exfoliation of graphite over SiO_x/Si wafer. After this, microcavities are etched through the graphite, SiO_x, and Si (see the Supporting Information for further fabrication details). Using an optical microscope,[40] we select graphite layers whose thicknesses ranged from ~10 to 30 nm. A custom-made transfer station is then used to transfer MoS_2 flakes over the etched graphite wells, thereby forming MoS_2 sealed microcavities (Figure 1b). Following the fabrication of both sets of devices, they are placed into a pressure chamber and charged to an input pressure (p_0) with argon gas. We wait ~48 h for gas to diffuse into the sealed microcavity such that the internal pressure (p_{int}) of the cavity and input pressure reach equilibrium ($p_0 = p_{int}$) before moving the devices to atmospheric pressure ($p_{ext} \equiv p_{atm} \approx 1$ atm), p_{int} is now larger than p_{ext} ($\Delta p = p_{int} - p_{ext} > 0$) and results in the MoS_2 membrane bulging upward, which we measure with an atomic force microscope (AFM) (Figure 1c). After each set of AFM measurements, the devices are placed back into the pressure chamber, which is set to a higher p_0, and the test is repeated (Figure 2a). Initially, the membrane's radius stays constant (a_0), which is the radius of the well, until a critical pressure is reached. Once the internal pressure exceeds this critical pressure, the membrane delaminates from the surface, overcoming the adhesion forces and creating a bulged blister. An AFM image of a bulged blister on a gold substrate showing the maximum deflection, δ, and radius, a, is shown in Figure 1d. (see the Supporting Information for the other tested substrates).

Utilizing Hencky's solution[41,42] for the deflection of a fully clamped circular membrane subjected to a pressure load Δp, we obtain the relationship between Δp and δ as

$$\Delta p = \frac{K(\nu)E_{2D}\delta^3}{a^4} \quad (1)$$

where E_{2D} is the two-dimensional Young's modulus and $K(\nu)$ is a constant which depends on the Poisson ratio (see the Supporting Information). For MoS_2, we use $K(\nu = 0.29) = 3.54$.[30] Figure 2b shows Δp vs $K(\nu)\delta^3/a^4$ for $a = a_0$. At each Δp, 3 AFM cross sections separated by ~10° and passing through the center are used to determine and average $K(\nu)\delta^3/a^4$ along with a standard deviation. A linear fit to the data is used to determine E_{2D} for each device (Figure 2c). The values of E_{2D} are consistent with monolayer or bilayer MoS_2. The scattering of E_{2D} values within the CVD-grown MoS_2 membranes may be caused by several factors such as the variations in the defect densities[43] and sulfur vacancies[44,45] from growth to growth, strain inhomogeneities which can be introduced during MoS_2 transfer over the wells,[46] and the possibility of bilayer flakes.

https://doi.org/10.1021/acs.nanolett.2c04886
Nano Lett. 2023, 23, 2607−2614

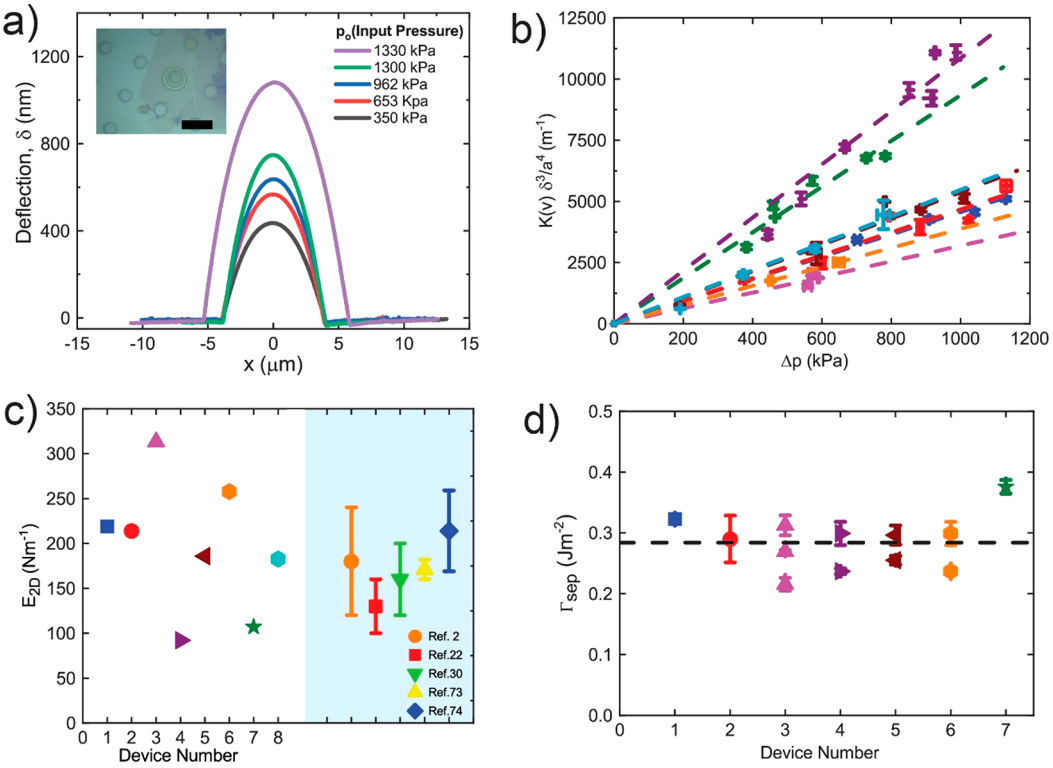

Figure 2. MoS_2 on a gold substrate. (a) AFM cross sections of the delaminated devices at various input pressure. Inset: optical image of the delaminated device over the gold substrate (the scale bar is 15 μm). (b) $K(\nu)\delta^3/a^4$ vs Δp for CVD-grown MoS_2 membranes. Dashed lines are linear fits used to calculate E_{2D} for each device. Different colors/symbols represent the different devices. (c) E_{2D} for each device in (b). Reference values are plotted for comparison.[2,22,30,73,74] (d) The corresponding E_{2D} for each device is used in the calculation of its work of separation. Several devices were subjected to multiple delaminations from the surface (one device got broken before delamination). Data points are the mean values, and the error bars represent the standard deviations. The dashed line is the average of all devices.

To determine the work of separation between the MoS_2 membrane and substrate, we use a previously developed free energy model[29,30,39] which assumes that the membrane, the membrane−substrate interface, the trapped gas, and the external atmosphere form an isothermal thermodynamic system whose free energy is given by

$$F = \frac{(p_{int} - p_{ext})V_b}{4} + \Gamma_{sep}\pi(a^2 - a_0^2) - p_0 V_0 \ln\left[\frac{V_0 + V_b}{V_0}\right] + p_{ext}V_b \quad (2)$$

where V_0 is the initial volume of the microcavity and V_b is the bulge volume that is created after the membrane expansion (see the Supporting Information). The terms on the right-hand side are (1) the strain energy of the membrane due to the pressure load, (2) the work of separation of the membrane from the substrate, where Γ_{sep} is the separation energy per unit area, (3) isothermal work done by the trapped gas in the microcavity, and (4) work of the external pressure. When the critical pressure is exceeded, the membrane delaminates from the surface, and the blister expands until the free energy reaches its minimum value. Using eq 2, we find the local minima of the free energy of the delaminated configuration by taking the derivative with respect to a and setting it to zero ($dF/da = 0$). Substituting eq 1 and the ideal gas law into the derivative yields

$$\Gamma_{sep} = \frac{5}{4}CKE_{2D}\left(\frac{\delta}{a}\right)^4 \quad (3)$$

where $C(\nu = 0.29) = 0.522$.[30] Using eq 3, we can determine the work of separation for devices showing delamination. For each delaminated device using the measured δ, a, and E_{2D} values of the corresponding devices (Figure 2c), we plot the mean values of Γ_{sep} for the 7 devices that delaminated over the gold substrates, with error bars representing the standard deviation. The standard deviation was calculated by averaging the deflection and radius of the delaminated device along 3 cross sections separated by ∼10°. Some devices are measured at several increasing values of p_0 and undergo multiple delaminations to larger delaminated radii, a, and these are shown as identically colored data points (Figure 2d). We find an average $\Gamma_{sep} = 0.28 \pm 0.04$ J/m^2 (Figure 2d), which agrees closely with previous work (0.27−0.67 J/m^2).[47] The difference in the work of separation within each device may be caused by several factors, including local roughness differences[48] due to the etching process of the wells where the rim of the well may be rougher than other nearby surfaces, carbon-based contamination on the surface,[12] or local differences in the chemical reactivity of the surface.[49] Measurements of strain-induced changes in photoluminescence (PL) of the MoS_2 membrane[25,50] confirm that the membrane remained well clamped to the substrate, thereby suggesting that Hencky's solution remains applicable throughout the delamination process (see the Supporting Information). As shown in the previous studies, the strain gets extended outside the well area; however, incorporating the extended strain into the regular Hencky solution has a minor effect (∼1% change) on the work of separation.[30,31,51] We repeat the same experiment on the other metal and Ge substrates and find values lower than those

https://doi.org/10.1021/acs.nanolett.2c04886
Nano Lett. 2023, 23, 2607−2614

of gold and SiO_x with a noticeable difference in separation energies among the metals and Ge substrate tested (Figure 3).

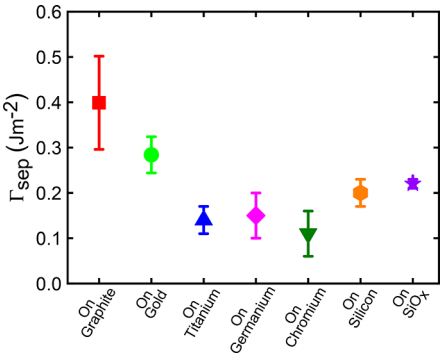

Figure 3. Comparison of work of separation among the graphite, Cr, Ti, Au, Ge, SiO_x, and Si substrates. Data points are mean values, and error bars represent the standard deviations.

Possible mechanisms for the variations in adhesion can be electrostatic interactions[52,53] resulting in different binding affinities[54−56] or a difference in surface roughness. It is notable that gold has the highest work function (5.47 eV) within our tested substrates and does not form a native oxide such as Ge and the other metals tested.

We also measure the adhesion of MoS_2 on graphite, a semimetal. The graphite surface is atomically smooth, assuming it is uncontaminated by surface residue and does not form a native oxide, though our graphite surfaces were slightly oxidized during processing (see the Supporting Information). We perform the blister test on 44 graphite devices (see the Supporting Information for further details). Figure 4a shows the mean values of Γ_{sep} for all of the MoS_2/graphite devices. As can be seen, almost all of the devices undergo multiple delaminations. We find an average Γ_{sep} = 0.39 ± 0.1 J/m^2, which is noticeably higher than that for the MoS_2 on gold devices (Γ_{sep} = 0.28 ± 0.04 J/m^2) and higher than that for the MoS_2 on SiO_x (Γ_{sep} = 0.22 ± 0.01 J/m^2) (Figure 3). A clear illustration of the difference in Γ_{sep} between MoS_2 on SiO_x and MoS_2 over the graphite substrate is seen in Figure 4b,c, where the MoS_2 is delaminated from the SiO_x to a larger radius but remains pinned to its original radius over the graphite well. This is due to the larger Γ_{sep} for MoS_2/graphite than for MoS_2/SiO_x.

One possibility for the differences in Γ_{sep} between MoS_2 and the metal or Ge substrates and graphite substrates is surface roughness. The surface roughness at the nanometer scale is critical to 2D material adhesion.[48,57,58] A freshly cleaved graphite surface should be atomically smooth and allow for better surface conformation[55,59,60] and perhaps better adhesion. Before the MoS_2 layers are transferred onto them, we find a graphite surface roughness of 0.21 ± 0.04 nm, which we attribute to photoresist contamination during processing. This roughness is similar to that of SiO_x (0.18 ± 0.01 nm) and slightly less than the roughnesses of the other metal or Ge surfaces (see Table S2 in the Supporting Information for the details). The aluminum substrate had the largest surface roughness (3.8 ± 0.8 nm), and we were unable to transfer MoS_2 onto it, which we attribute to this large surface roughness, suggesting that surface roughness may play a role in our adhesion measurements. This suggests that the aluminum has a small work of adhesion. However, without higher-resolution imaging of the surface such as that enabled by a scanning tunneling microscope, we are limited in the conclusion we can draw (see movies 1−4 in the Supporting Information for the transfer videos).

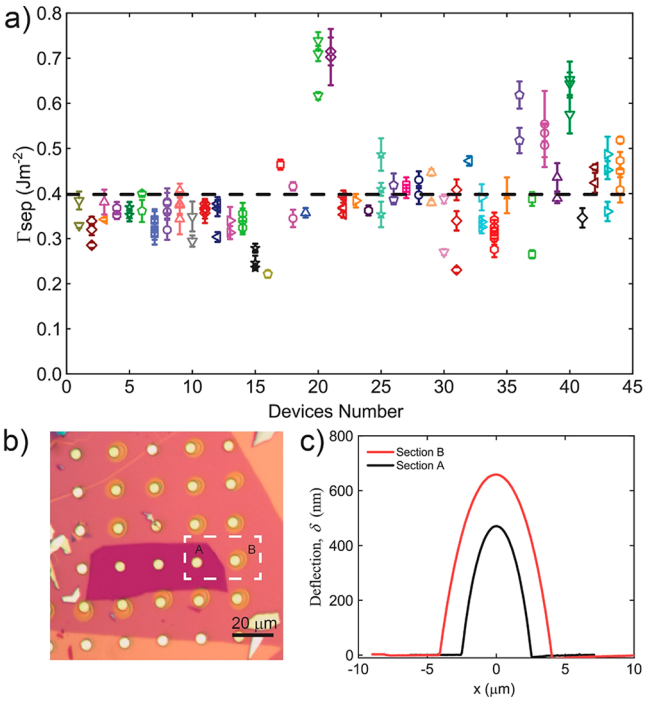

Figure 4. (a) Work of separation for the graphite devices. Most of the devices were subjected to multiple delaminations from the surface. Data points are mean values, and the error bars represent the standard deviations. The dashed line is the average of all devices. (b) Optical image of MoS_2 over graphite. (c) Cross sections of the devices labeled with the dashed line in (b) at the same input pressure. The membrane over the SiO_x shows earlier delamination due to a lower work of separation.

Another mechanism for adhesion differences is the work function difference and chemical bonding between the 2D material and the substrate. Previously, it was shown that MoS_2 is more readily exfoliated onto freshly prepared gold substrates presumably due to a sulfur−gold bond that forms.[55] This could explain the larger adhesion we observe for gold over the other metals and Ge. Titanium, Cr, and Ge had similar surface roughnesses and correspondingly similar adhesions. They also all form a native oxide. Further studies are needed to confirm the exact roles that surface roughness, work function differences, and chemical bonding play in determining surface adhesion between 2D materials and their substrates.

In addition to measuring Γ_{sep}, we also measure the work of adhesion, Γ_{adh}. To do so, each device is monitored in the AFM under ambient conditions after delamination. Both the deflection and radius are continuously measured in the AFM over a period of 24 h to 10 days. As gas slowly leaks out of the well, the deflection decreases, but the radius stays pinned at the delaminated radius (Figure 5a). Once the deflection reaches a critical height, we see a gradual decrease in both the radius and the height of the blister.

In Figure 5b, we plot δ vs a for MoS_2 on gold and graphite samples undergoing both delamination and relamination. This difference in paths between delamination and relamination is attributed to adhesion hysteresis[61] similar to what we

https://doi.org/10.1021/acs.nanolett.2c04886
Nano Lett. 2023, 23, 2607−2614

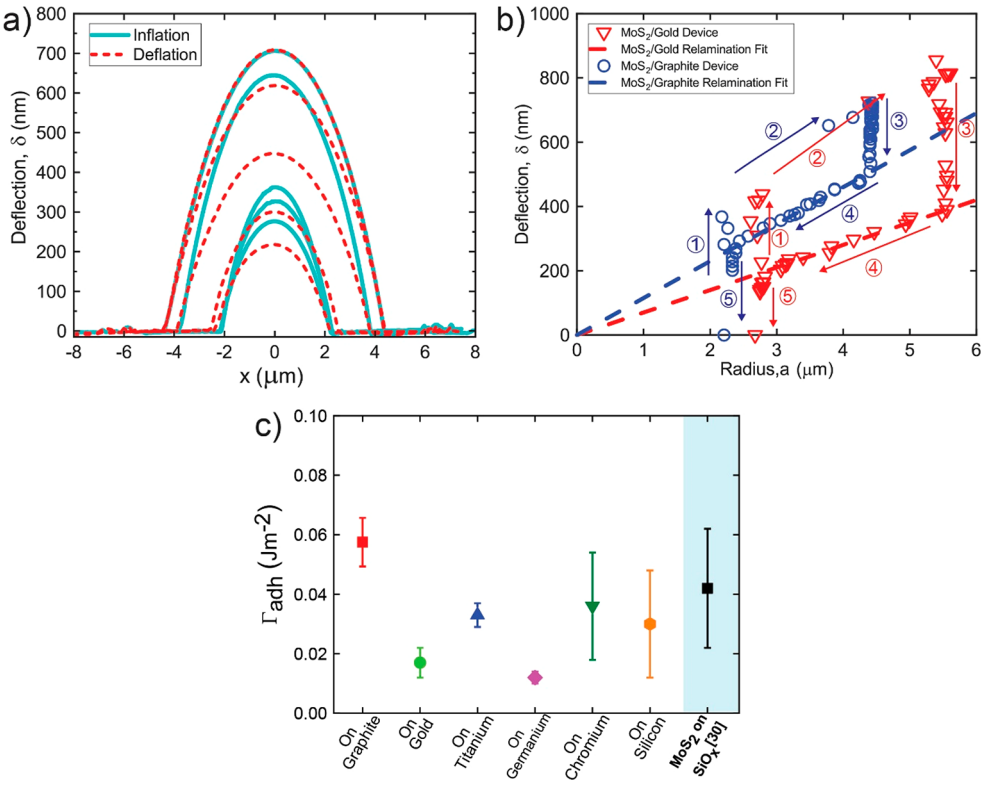

Figure 5. (a) AFM cross-section of the device during inflation and deflation. (b) δ and a during the inflation and deflation. Gold and graphite substrates are shown (see the Supporting Information for more data). Arrows show various regimes: (1) inflation, (2) separation, (3) deflation at a pinned radius, (4) relamination, and (5) deflation at the well's radius. Dashed lines are the linear fits for the calculation of the work of adhesion. (c) Comparison of the work of adhesion among graphite, Au, Ti, Ge, Cr, and Si substrates. Data points are mean values, and error bars represent the standard deviation.

previously observed in MoS_2 on SiO_x[30,62,63] (see the Supporting Information for the other tested substrates).

Using a modified version of eq 3, we determine Γ_{adh}.[30] The onset of the relamination occurs at the critical deflection, δ_c. The relamination process then takes place along a line where the slope is given by Γ_{adh}. The expression for the relamination energy can then be written as

$$\Gamma_{adh} = \frac{5}{4} CKE_{2D} \left(\frac{\delta_c}{a_d} \right)^4 \quad (4)$$

where δ_c is the critical deflection and a_d the radius at this deflection. Comparing Figures 3 and 5c, the energy that separates the membrane from the surface is considerably higher than the energy the membrane recovers upon relamination ($\Gamma_{sep} > \Gamma_{adh}$). We find that Γ_{adh} ranged from $\Gamma_{adh} = 0.057 \pm 0.008$ J/m^2 for graphite devices to $\Gamma_{adh} = 0.01 \pm 0.002$ J/m^2 for germanium devices (Figure 5c). (see the Supporting Information for complete data sets). This adhesion hysteresis was similar to what was previously observed in MoS_2 on SiO_x.[30]

The exact mechanism for the hysteresis is not fully comprehended, but one possible reason is that the membrane−substrate interface formed during the relamination is not equivalent to that which is broken during delamination. However, during pressurizing of the microcavities to p_0 the external pressure applied may alter the membrane−substrate interface by pushing the membrane onto the substrate and thereby increase the adhesive interactions prior to delamination measurements.[64−70]

In conclusion, we measured the work of separation of MoS_2 to graphite, Ge, Cr, Ti, and Au substrates using a blister test. We found Γ_{sep} ranging from 0.08 ± 0.03 J/m^2 for Cr to 0.39 ± 0.1 J/m^2 for graphite substrates and a Γ_{adh} value considerably lower than the Γ_{sep} value. Our results suggest that both surface roughness and chemical interactions may play a role in the surface adhesion of 2D materials, but more research is needed to conclusively determine the exact contribution each makes. A measurement of both the work of separation and adhesion for a range of substrates as provided here is critical to guiding the future design of electrical and mechanical devices based on 2D materials due to the prominent role that these adhesive surfaces play in their fabrication and functionality.[18,71,72]

■ ASSOCIATED CONTENT

Supporting Information

Supporting Information covers the and videos of . The Supporting Information is available free of charge at https://pubs.acs.org/doi/10.1021/acs.nanolett.2c04886.

CVD growth and characterization, metal, Ge, and graphite fabrication procedures, MoS_2 transfer method to substrates, graphite surface treatment, photoluminescence verification for clamping conditions, data sets of graphite Young's modulus calculation, relamination data sets for metal, Ge, and graphite substrates, and surface roughness examination (PDF)

MoS_2 transfer to SiO_x substrate (MP4)

MoS_2 transfer to Cr substrate (MP4)

MoS_2 transfer to Ti substrate (MP4)

MoS_2 transfer to Al substrate (MP4)

https://doi.org/10.1021/acs.nanolett.2c04886
Nano Lett. 2023, 23, 2607−2614

AUTHOR INFORMATION

Corresponding Author

J. Scott Bunch − *Boston University, Department of Mechanical Engineering, Boston, Massachusetts 02215, United States; Boston University, Division of Materials Science and Engineering, Brookline, Massachusetts 02446, United States;* Email: bunch@bu.edu

Authors

Metehan Calis − *Boston University, Department of Mechanical Engineering, Boston, Massachusetts 02215, United States;* orcid.org/0009-0007-1033-2438

David Lloyd − *Analog Garage, Analog Devices Inc., Boston, Massachusetts 02110, United States*

Narasimha Boddeti − *Washington State University, School of Mechanical and Materials Engineering, Pullman, Washington 99163, United States*

Complete contact information is available at: https://pubs.acs.org/10.1021/acs.nanolett.2c04886

Notes

The authors declare no competing financial interest.

ACKNOWLEDGMENTS

This work was funded by the Ministry of National Education of Turkey under the Graduate Education Scholarship (YLSY) program.

REFERENCES

(1) Novoselov, K. S.; Geim, A. K.; Morozov, S. V.; Jiang, D.; Zhang, Y.; Dubonos, S. V.; Grigorieva, I. V.; Firsov, A. A. Electric Field in Atomically Thin Carbon Films. *Science (80-.)* **2004**, *306* (5696), 666−669.

(2) Bertolazzi, S.; Brivio, J.; Kis, A. Stretching and Breaking of Ultrathin MoS 2. *ACS Nano* **2011**, *5* (12), 9703−9709.

(3) Lee, C.; Wei, X.; Kysar, J. W.; Hone, J. Measurement of the Elastic Properties and Intrinsic Strength of Monolayer Graphene. *Science (80-.)* **2008**, *321* (5887), 385−388.

(4) Geim, A. K. Graphene: Status and Prospects. *Science* **2009**, *324*, 1530−1534.

(5) Sun, P. Z.; Yang, Q.; Kuang, W. J.; Stebunov, Y. V.; Xiong, W. Q.; Yu, J.; Nair, R. R.; Katsnelson, M. I.; Yuan, S. J.; Grigorieva, I. V.; Lozada-Hidalgo, M.; Wang, F. C.; Geim, A. K. Limits on Gas Impermeability of Graphene. *Nature* **2020**, *579* (7798), 229−232.

(6) Bunch, J. S.; Verbridge, S. S.; Alden, J. S.; Van Der Zande, A. M.; Parpia, J. M.; Craighead, H. G.; McEuen, P. L. Impermeable Atomic Membranes from Graphene Sheets. *Nano Lett.* **2008**, *8* (8), 2458−2462.

(7) Lindsay, L.; Broido, D. A. Enhanced Thermal Conductivity and Isotope Effect in Single-Layer Hexagonal Boron Nitride. *Phys. Rev. B - Condens. Matter Mater. Phys.* **2011**, *84* (15), 155421.

(8) Zhang, G.; Zhang, Y. W. Thermoelectric Properties of Two-Dimensional Transition Metal Dichalcogenides. *J. Mater. Chem. C* **2017**, *5* (31), 7684−7698.

(9) Bolotin, K. I.; Sikes, K. J.; Jiang, Z.; Klima, M.; Fudenberg, G.; Hone, J.; Kim, P.; Stormer, H. L. Ultrahigh Electron Mobility in Suspended Graphene. *Solid State Commun.* **2008**, *146* (9−10), 351−355.

(10) Kim, S.; Konar, A.; Hwang, W. S.; Lee, J. H.; Lee, J.; Yang, J.; Jung, C.; Kim, H.; Yoo, J. B.; Choi, J. Y.; Jin, Y. W.; Lee, S. Y.; Jena, D.; Choi, W.; Kim, K. High-Mobility and Low-Power Thin-Film Transistors Based on Multilayer MoS2 Crystals. *Nat. Commun.* **2012**, *3* (1), 1−7.

(11) Peng, Z.; Chen, X.; Fan, Y.; Srolovitz, D. J.; Lei, D. Strain Engineering of 2D Semiconductors and Graphene: From Strain Fields to Band-Structure Tuning and Photonic Applications. *Light Sci. Appl.* **2020**, *9* (1), 1−25.

(12) Choi, W.; Choudhary, N.; Han, G. H.; Park, J.; Akinwande, D.; Lee, Y. H. Recent Development of Two-Dimensional Transition Metal Dichalcogenides and Their Applications. *Mater. Today* **2017**, *20* (3), 116−130.

(13) Liu, Y.; Huang, Y.; Duan, X. Van Der Waals Integration before and beyond Two-Dimensional Materials. *Nature* **2019**, *567* (7748), 323−333.

(14) Buscema, M.; Island, J. O.; Groenendijk, D. J.; Blanter, S. I.; Steele, G. A.; Van Der Zant, H. S. J.; Castellanos-Gomez, A. Photocurrent Generation with Two-Dimensional van Der Waals Semiconductors. *Chem. Soc. Rev.* **2015**, *44* (11), 3691−3718.

(15) Geim, A. K.; Grigorieva, I. V. Van Der Waals Heterostructures. *Nature* **2013**, *499* (7459), 419−425.

(16) Dean, C. R.; Young, A. F.; Meric, I.; Lee, C.; Wang, L.; Sorgenfrei, S.; Watanabe, K.; Taniguchi, T.; Kim, P.; Shepard, K. L.; Hone, J. Boron Nitride Substrates for High-Quality Graphene Electronics. *Nat. Nanotechnol.* **2010**, *5* (10), 722−726.

(17) Ye, F.; Lee, J.; Feng, P. X. L. Atomic Layer MoS2-Graphene van Der Waals Heterostructure Nanomechanical Resonators. *Nanoscale* **2017**, *9* (46), 18208−18215.

(18) Britnell, L.; Ribeiro, R. M.; Eckmann, A.; Jalil, R.; Belle, B. D.; Mishchenko, A.; Kim, Y. J.; Gorbachev, R. V.; Georgiou, T.; Morozov, S. V.; Grigorenko, A. N.; Geim, A. K.; Casiraghi, C.; Castro Neto, A. H.; Novoselov, K. S. Strong Light-Matter Interactions in Heterostructures of Atomically Thin Films. *Science (80-.)* **2013**, *340* (6138), 1311−1314.

(19) Ye, F.; Islam, A.; Zhang, T.; Feng, P. X. L. Ultrawide Frequency Tuning of Atomic Layer van Der Waals Heterostructure Electromechanical Resonators. *Nano Lett.* **2021**, *21* (13), 5508−5515.

(20) Liu, Y.; Xu, Z.; Zheng, Q. The Interlayer Shear Effect on Graphene Multilayer Resonators. *J. Mech. Phys. Solids* **2011**, *59* (8), 1613−1622.

(21) Li, B.; Yin, J.; Liu, X.; Wu, H.; Li, J.; Li, X.; Guo, W. Probing van Der Waals Interactions at Two-Dimensional Heterointerfaces. *Nat. Nanotechnol.* **2019**, *14* (6), 567−572.

(22) Cooper, R. C.; Lee, C.; Marianetti, C. A.; Wei, X.; Hone, J.; Kysar, J. W. Nonlinear Elastic Behavior of Two-Dimensional Molybdenum Disulfide. *Phys. Rev. B - Condens. Matter Mater. Phys.* **2013**, *87* (3), 035423.

(23) Sharma, M.; Singh, A.; Singh, R. Monolayer MoS2Transferred on Arbitrary Substrates for Potential Use in Flexible Electronics. *ACS Appl. Nano Mater.* **2020**, *3* (5), 4445−4453.

(24) Splendiani, A.; Sun, L.; Zhang, Y.; Li, T.; Kim, J.; Chim, C. Y.; Galli, G.; Wang, F. Emerging Photoluminescence in Monolayer MoS2. *Nano Lett.* **2010**, *10* (4), 1271−1275.

(25) Lloyd, D.; Liu, X.; Christopher, J. W.; Cantley, L.; Wadehra, A.; Kim, B. L.; Goldberg, B. B.; Swan, A. K.; Bunch, J. S. Band Gap Engineering with Ultralarge Biaxial Strains in Suspended Monolayer MoS2. *Nano Lett.* **2016**, *16* (9), 5836−5841.

(26) Rokni, H.; Lu, W. Direct Measurements of Interfacial Adhesion in 2D Materials and van Der Waals Heterostructures in Ambient Air. *Nat. Commun.* **2020**, *11* (1), 1−14.

(27) Fang, Z.; Li, X.; Shi, W.; Li, Z.; Guo, Y.; Chen, Q.; Peng, L.; Wei, X. Interlayer Binding Energy of Hexagonal MoS2as Determined by an in Situ Peeling-to-Fracture Method. *J. Phys. Chem. C* **2020**, *124* (42), 23419−23425.

(28) Wan, K. T.; Mai, Y. W. Fracture Mechanics of a New Blister Test with Stable Crack Growth. *Acta Metall. Mater.* **1995**, *43* (11), 4109−4115.

(29) Boddeti, N. G.; Koenig, S. P.; Long, R.; Xiao, J.; Bunch, J. S.; Dunn, M. L. Mechanics of Adhered, Pressurized Graphene Blisters. *J. Appl. Mech. Trans. ASME* **2013**, *80* (4), 040909 DOI: 10.1115/1.4024255.

(30) Lloyd, D.; Liu, X.; Boddeti, N.; Cantley, L.; Long, R.; Dunn, M. L.; Bunch, J. S. Adhesion, Stiffness, and Instability in Atomically Thin MoS2 Bubbles. *Nano Lett.* **2017**, *17* (9), 5329−5334.

(31) Wang, G.; Dai, Z.; Wang, Y.; Tan, P.; Liu, L.; Xu, Z.; Wei, Y.; Huang, R.; Zhang, Z. Measuring Interlayer Shear Stress in Bilayer Graphene. *Phys. Rev. Lett.* **2017**, *119* (3), 036101.
(32) Kitt, A. L.; Qi, Z.; Rémi, S.; Park, H. S.; Swan, A. K.; Goldberg, B. B. How Graphene Slides: Measurement and Theory of Strain-Dependent Frictional Forces between Graphene and SiO2. *Nano Lett.* **2013**, *13* (6), 2605−2610.
(33) Huang, C.; Jin, Y.; Wang, W.; Tang, L.; Song, C.; Xiu, F. Manganese and Chromium Doping in Atomically Thin MoS2. *J. Semicond.* **2017**, *38* (3), 033004.
(34) Andzane, J.; Petkov, N.; Livshits, A. I.; Boland, J. J.; Holmes, J. D.; Erts, D. Two-Terminal Nanoelectromechanical Devices Based on Germanium Nanowires. *Nano Lett.* **2009**, *9* (5), 1824−1829.
(35) Zhao, X.; Yang, S.; Sun, Z.; Cui, N.; Zhao, P.; Tang, Q.; Tong, Y.; Liu, Y. Enhancing the Intrinsic Stretchability of Micropatterned Gold Film by Covalent Linkage of Carbon Nanotubes for Wearable Electronics. *ACS Appl. Electron. Mater.* **2019**, *1* (7), 1295−1303.
(36) Abbasi, N. M.; Xiao, Y.; Zhang, L.; Peng, L.; Duo, Y.; Wang, L.; Yin, P.; Ge, Y.; Zhu, H.; Zhang, B.; Xie, N.; Duan, Y.; Wang, B.; Zhang, H. Heterostructures of Titanium-Based MXenes in Energy Conversion and Storage Devices. *J. Mater. Chem. C* **2021**, *9* (27), 8395−8465.
(37) Lemme, M. C.; Wagner, S.; Lee, K.; Fan, X.; Verbiest, G. J.; Wittmann, S.; Lukas, S.; Dolleman, R. J.; Niklaus, F.; van der Zant, H. S. J.; Duesberg, G. S.; Steeneken, P. G. Nanoelectromechanical Sensors Based on Suspended 2D Materials. *Research* **2020**, *2020*, 1−25.
(38) Frisenda, R.; Niu, Y.; Gant, P.; Muñoz, M.; Castellanos-Gomez, A. Naturally Occurring van Der Waals Materials. *npj 2D Mater. Appl.* **2020**, *4* (1), 1−13.
(39) Koenig, S. P.; Boddeti, N. G.; Dunn, M. L.; Bunch, J. S. Ultrastrong Adhesion of Graphene Membranes. *Nat. Nanotechnol.* **2011**, *6* (9), 543−546.
(40) Li, H.; Wu, J.; Huang, X.; Lu, G.; Yang, J.; Lu, X.; Xiong, Q.; Zhang, H. Rapid and Reliable Thickness Identification of Two-Dimensional Nanosheets Using Optical Microscopy. *ACS Nano* **2013**, *7* (11), 10344−10353.
(41) Fichter, W. B. Some Solutions for the Large Deflections of Uniformly Loaded Circular Membranes. *NASA Technol. Pap.* **1997**, *3658*, 1−24.
(42) Hencky, H. Ueber Den Spannungszustand in Kreisrunden Platten Mit Verschwindender Biegungssteifigkeit. *Zeitschrift für Math. und Phys.* **1915**, *63*, 311−317.
(43) Zandiatashbar, A.; Lee, G. H.; An, S. J.; Lee, S.; Mathew, N.; Terrones, M.; Hayashi, T.; Picu, C. R.; Hone, J.; Koratkar, N. Effect of Defects on the Intrinsic Strength and Stiffness of Graphene. *Nat. Commun.* **2014**, *5* (1), 1−9.
(44) Hong, J.; Hu, Z.; Probert, M.; Li, K.; Lv, D.; Yang, X.; Gu, L.; Mao, N.; Feng, Q.; Xie, L.; Zhang, J.; Wu, D.; Zhang, Z.; Jin, C.; Ji, W.; Zhang, X.; Yuan, J.; Zhang, Z. Exploring Atomic Defects in Molybdenum Disulphide Monolayers. *Nat. Commun.* **2015**, *6* (1), 1−8.
(45) Gan, Y.; Zhao, H. Chirality Effect of Mechanical and Electronic Properties of Monolayer MoS2 with Vacancies. *Phys. Lett. A* **2014**, *378* (38−39), 2910−2914.
(46) Liu, B.; Pavlou, C.; Wang, Z.; Cang, Y.; Galiotis, C.; Fytas, G. Determination of the Elastic Moduli of CVD Graphene by Probing Graphene/Polymer Bragg Stacks. *2D Mater.* **2021**, *8* (3), 035040.
(47) Fang, Z.; Dai, Z.; Wang, B.; Tian, Z.; Yu, C.; Chen, Q.; Wei, X. Pull-to-Peel of Two-Dimensional Materials for the Simultaneous Determination of Elasticity and Adhesion. *Nano Lett.* **2022**, *23*, 742.
(48) Boddeti, N. G.; Long, R.; Dunn, M. L. Adhesion Mechanics of Graphene on Textured Substrates. *Int. J. Solids Struct.* **2016**, *97* (98), 56−74.
(49) Liu, X.; Boddeti, N. G.; Szpunar, M. R.; Wang, L.; Rodriguez, M. A.; Long, R.; Xiao, J.; Dunn, M. L.; Bunch, J. S. Observation of Pull-in Instability in Graphene Membranes under Interfacial Forces. *Nano Lett.* **2013**, *13* (5), 2309−2313.
(50) Yang, R.; Lee, J.; Ghosh, S.; Tang, H.; Sankaran, R. M.; Zorman, C. A.; Feng, P. X. L. Tuning Optical Signatures of Single- and Few-Layer MoS2 by Blown-Bubble Bulge Straining up to Fracture. *Nano Lett.* **2017**, *17* (8), 4568−4575.
(51) Ma, Y.; Wang, G.; Chen, Y.; Long, D.; Guan, Y.; Liu, L.; Zhang, Z. Extended Hencky Solution for the Blister Test of Nanomembrane. *Extrem. Mech. Lett.* **2018**, *22*, 69−78.
(52) Vernov, A.; Steele, W. A. The Electrostatic Field at a Graphite Surface and Its Effect on Molecule-Solid Interactions. *Langmuir* **1992**, *8* (1), 155−159.
(53) Speake, C. C.; Trenkel, C. Forces between Conducting Surfaces Due to Spatial Variations of Surface Potential. *Phys. Rev. Lett.* **2003**, *90* (16), 4.
(54) Velický, M.; Rodriguez, A.; Bouša, M.; Krayev, A. V.; Vondráček, M.; Honolka, J.; Ahmadi, M.; Donnelly, G. E.; Huang, F.; Abrunã, H. D.; Novoselov, K. S.; Frank, O. Strain and Charge Doping Fingerprints of the Strong Interaction between Monolayer MoS2and Gold. *J. Phys. Chem. Lett.* **2020**, *11* (15), 6112−6118.
(55) Velický, M.; Donnelly, G. E.; Hendren, W. R.; McFarland, S.; Scullion, D.; DeBenedetti, W. J. I.; Correa, G. C.; Han, Y.; Wain, A. J.; Hines, M. A.; Muller, D. A.; Novoselov, K. S.; Abruña, H. D.; Bowman, R. M.; Santos, E. J. G.; Huang, F. Mechanism of Gold-Assisted Exfoliation of Centimeter-Sized Transition-Metal Dichalcogenide Monolayers. *ACS Nano* **2018**, *12* (10), 10463−10472.
(56) Chen, X.; Tian, F.; Persson, C.; Duan, W.; Chen, N. X. Interlayer Interactions in Graphites. *Sci. Reports* **2013**, *3* (1), 1−5.
(57) Aitken, Z. H.; Huang, R. Effects of Mismatch Strain and Substrate Surface Corrugation on Morphology of Supported Monolayer Graphene. *J. Appl. Phys.* **2010**, *107* (12), 123531.
(58) Gao, W.; Huang, R. Effect of Surface Roughness on Adhesion of Graphene Membranes. *J. Phys. D. Appl. Phys.* **2011**, *44* (45), 452001.
(59) Xin, H.; Borduin, R.; Jiang, W.; Liechti, K. M.; Li, W. Adhesion Energy of As-Grown Graphene on Copper Foil with a Blister Test. *Carbon N. Y.* **2017**, *123*, 243−249.
(60) Gao, W.; Huang, R. Effect of Surface Roughness on Adhesion of Graphene Membranes. *J. Phys. D. Appl. Phys.* **2011**, *44* (45), 452001.
(61) Kesari, H.; Doll, J. C.; Pruitt, B. L.; Cai, W.; Lew, A. J. Role of Surface Roughness in Hysteresis during Adhesive Elastic Contact. *Philos. Mag. Lett.* **2010**, *90* (12), 891−902.
(62) Miskin, M. Z.; Sun, C.; Cohen, I.; Dichtel, W. R.; McEuen, P. L. Measuring and Manipulating the Adhesion of Graphene. *Nano Lett.* **2018**, *18* (1), 449−454.
(63) Chen, Y. L.; Helm, C. A.; Israelachvili, J. N. Molecular Mechanisms Associated with Adhesion and Contact Angle Hysteresis of Monolayer Surfaces. *J. Phys. Chem.* **1991**, *95* (26), 10736−10747.
(64) Girard-Reydet, E.; Oslanec, R.; Whitten, P.; Brown, H. R. Effects of Contact Time and Polarity Level on Adhesion between Interacting Surfaces. *Langmuir* **2004**, *20* (3), 708−713.
(65) Maugis, D.; Barquins, M. Fracture Mechanics and the Adherence of Viscoelastic Bodies. *J. Phys. D. Appl. Phys.* **1978**, *11* (14), 1989.
(66) Suk, J. W.; Na, S. R.; Stromberg, R. J.; Stauffer, D.; Lee, J.; Ruoff, R. S.; Liechti, K. M. Probing the Adhesion Interactions of Graphene on Silicon Oxide by Nanoindentation. *Carbon N. Y.* **2016**, *103*, 63−72.
(67) Kim, S.; Choi, G. Y.; Ulman, A.; Fleischer, C. Effect of Chemical Functionality on Adhesion Hysteresis. *Langmuir* **1997**, *13* (25), 6850−6856.
(68) Makkonen, L. A. Thermodynamic Model of Contact Angle Hysteresis. *J. Chem. Phys.* **2017**, *147* (6), 064703.
(69) Kang, J.; Sahin, H.; Peeters, F. M. Mechanical Properties of Monolayer Sulphides: A Comparative Study between MoS2, HfS2 and TiS3. *Phys. Chem. Chem. Phys.* **2015**, *17* (41), 27742−27749.
(70) Qiao, S.; Gratadour, J. B.; Wang, L.; Lu, N. Conformability of a Thin Elastic Membrane Laminated on a Rigid Substrate With Corrugated Surface. *IEEE Trans. Components, Packag. Manuf. Technol.* **2015**, *5* (9), 1237−1243.

https://doi.org/10.1021/acs.nanolett.2c04886
Nano Lett. 2023, 23, 2607−2614

(71) Furchi, M. M.; Höller, F.; Dobusch, L.; Polyushkin, D. K.; Schuler, S.; Mueller, T. Device Physics of van Der Waals Heterojunction Solar Cells. *npj 2D Mater. Appl.* **2018**, *2* (1), 1−7.
(72) Bediako, D. K.; Rezaee, M.; Yoo, H.; Larson, D. T.; Zhao, S. Y. F.; Taniguchi, T.; Watanabe, K.; Brower-Thomas, T. L.; Kaxiras, E.; Kim, P. Heterointerface Effects in the Electrointercalation of van Der Waals Heterostructures. *Nature* **2018**, *558* (7710), 425−429.
(73) Liu, K.; Yan, Q.; Chen, M.; Fan, W.; Sun, Y.; Suh, J.; Fu, D.; Lee, S.; Zhou, J.; Tongay, S.; Ji, J.; Neaton, J. B.; Wu, J. Elastic Properties of Chemical-Vapor-Deposited Monolayer MoS2, WS2, and Their Bilayer Heterostructures. *Nano Lett.* **2014**, *14* (9), 5097−5103.
(74) Castellanos-Gomez, A.; Poot, M.; Steele, G. A.; Van Der Zant, H. S. J.; Agraït, N.; Rubio-Bollinger, G. Elastic Properties of Freely Suspended MoS2 Nanosheets. *Adv. Mater.* **2012**, *24* (6), 772−775.

https://doi.org/10.1021/acs.nanolett.2c04886
Nano Lett. 2023, 23, 2607−2614